



# Influence of Thermal Processing Conditions on Mechanical and Material Properties of 3D Printed Thin-Structures Using PEEK Material

Han Qu<sup>1</sup> · Wei Zhang<sup>1</sup> · Zihan Li<sup>1</sup> · Liyao Hou<sup>1</sup> · Guiwei Li<sup>1</sup> · Jerry YH Fuh<sup>2</sup> · Wenzheng Wu<sup>1</sup>

Received: 29 July 2021 / Revised: 24 March 2022 / Accepted: 6 April 2022 / Published online: 9 May 2022  
© The Author(s), under exclusive licence to Korean Society for Precision Engineering 2022

## Abstract

Poly-ether-ether-ketone (PEEK) was one of the most promising engineering plastics, which had been widely employed in the aerospace, biomedical and automotive industry and manufacturing. The design of various 3D printing (3DP) parameters had a significant impact on its mechanical and thermal properties. This study aimed to investigate the thermodynamic properties of thin-structure PEEK samples by printing them under various conditions, including varying substrate and ambient temperature parameters, under a control- method. Numerous critical properties such as interlayer bonding force, tensile and bending properties, dynamic mechanical properties, and crystallization had been investigated in this work. The results indicated that the maximum relative interlayer bonding force was 989.91 N, while comparing to the lowest initial ambient and substrate temperature 60 °C and 90 °C, the optimal tensile and bending strengths both increased by 28.46% and 13.86% to 86.62 MPa and 113.21 MPa under ambient and substrate temperature 90 °C and 160 °C, respectively. Concurrently, the crystallinity increased by 6.67% to 31.56%. Mechanical and thermal properties had been significantly improved when appropriate substrate temperature parameters were used during the printing process, demonstrating the enormous potential in printing PEEK material. Thermal processing was another critical factor in achieving higher performance of 3D printing PEEK components.

**Keywords** FFF · 3D printing · PEEK · Thermal processing · Mechanical properties

## 1 Introduction

Compared with traditional subtractive processing technologies, additive manufacturing (AM) was a novel manufacturing method in which materials were accumulated layer by layer using discrete-accumulation principle, overcoming the constraint of traditional manufacturing on complex internal geometry. Fused filament fabrication (FFF) was the most frequently used AM method in thermoplastic printing. Since FFF technology had a simple structure, low maintenance cost, high utilization advantages, it was widely used in additive manufacturing of low strength polymers such as ABS

[1] and PLA [2], as well as high-performance engineering plastics, such as PEI [3, 4], TPI [5], PPS [6], PEEK [7–22], etc. Recent advances in research had resulted in the publication of novel studies incorporating functional particles such as fiber-reinforced [7–9], GNT [10], carbon nanotubes [10, 11], silver nanowire [12], and SiO<sub>2</sub> [13, 22].

Poly-ether-ether-ketone (PEEK) was a well-known semi-crystalline high-molecular polymer that had been hailed as the most potential alternative material to replace low-performance metals due to its high-temperature and chemical corrosion resistance, as well as its unique mechanical properties, resulting in great promise in automobile manufacturing, biomedical [14, 15], food processing, aerospace and electric manufacturing [10]. In recent years, PEEK had recently received increased attention in AM technology. Compared with conventional injection molding, FFF [16] and SLS [17] were proved to be the best methods to construct flexible geometry and arbitrary intricate profiles. Whereas SLS method was characterized by lower material utilization and higher equipment cost, it had been demonstrated that FFF method was more economical in printing PEEK, and the relevant manufacturing

✉ Wenzheng Wu  
wzwu@jlu.edu.cn

<sup>1</sup> Advanced Materials Additive Manufacturing (AM)<sup>2</sup> Lab, School of Mechanical and Aerospace Engineering, Jilin University, Changchun 130025, Jilin, People's Republic of China

<sup>2</sup> Department of Mechanical Engineering, National University of Singapore, Singapore 117576, Singapore

processes and printing equipment [18, 19] had been recently published. In 2015, Wu et al. [1] published the first research on PEEK printing using FFF, examining the effect of layer thickness and raster angle on mechanical properties and testing the maximum tensile strength of 56 MPa. Hu et al. [18] reported an optimized new print head structure with a heat collection, significantly reducing the warpage and delamination during PEEK printing. Ding et al. [19] investigated the influence of nozzle temperature and printing orientation on PEEK's mechanical properties and microscopic morphology. They discovered that 80% of injection molding parts had less internal defects when nozzle temperature was increased. It was found that when the printing orientation was parallel to the load direction, the optimal bending and impact strength was obtained. Wang et al. [20] compared the performance of three different printer brands and investigated the ambient temperature and annealing treatment, proposing the importance of improving the testing standards for products and equipment under FDA regulations. Yang et al. [21] successfully increased the crystallization rate by about 16% by varying the ambient temperature from 25 to 200 °C and found that the furnace cooling and annealing methods could remarkably increase crystallinity to 36% and 38%, respectively. The temperature control had a meaningful impact on PEEK's mechanical properties. Vaezi et al. [22] reported a simple homemade heating device, which integrated two heating lamps and a heating substrate to precisely control the temperature during printing process. Research indicated that heat control during printing could ensure the interlayer bonding performance, thus avoiding warping and delamination.

Obviously, previous studies had demonstrated that temperature had a significant influence on geometric morphology, crystallinity, mechanical and thermal properties of PEEK simples. Although they had been studied on this fields, but the shortcoming was that there's no quantitative specific experiment for ambient and substrate temperature. Accordingly, our purpose was to explore and quantify the effects of ambient and substrate temperatures on cross-section morphology, interlayer bonding force, crystallinity, mechanical (tensile and bending), and dynamic mechanical properties of thin-thickness structures printed with pure PEEK material. Even if the conclusions were limited by the printer, but this was the first study that carried out quantitative analysis for the temperature of ambient and substrate parameters simultaneously.

## 2 Materials and Methods

### 2.1 Materials and FFF Equipment

Commercial ZYPEEK powder\_550G (Jilin Joinature Polymer Co., Ltd, Changchun, China) was used to extrude

1.75 mm ± 0.02 mm PEEK filament by a customized twin-screw extruder (CTE Coperion GmbH, Nanjing, China). Due to PEEK's susceptibility to water absorption, both powder and filament were dried in a vacuum drying oven (DZF-1, Ever Bright Medical Treatment Instrument Co., Ltd, Beijing, China) at 160 °C for 4 h and then vacuum-packaged before printing. All samples were printed with the same material by FUNMAT HT (Intamsys Technology Co., Ltd, Shanghai, China). The maximum load capacity of ambient and bed temperatures were 90 °C and 160 °C, respectively. To verify the thermal influence on printing samples, we should combine with the actual usage of the equipment. The experiment was divided into two groups. The first group used a constant bed temperature of 160 °C, and thus the parameters of a representative ambient temperature range of 60–90 °C were selected (the ambient temperature cannot fall below 60 °C because of the limitation of printer). In the second group, the selected representative bed temperature were from 90 to 160 °C in a constant ambient temperature of 90 °C. CATIA V5 software was utilized to draft the models and import STL files into IntamSuite software (Intamsys Technology Co., Ltd, Shanghai, China) to generate the sliced gcode. Table 1 summarized the detailed selected parameters of PEEK samples.

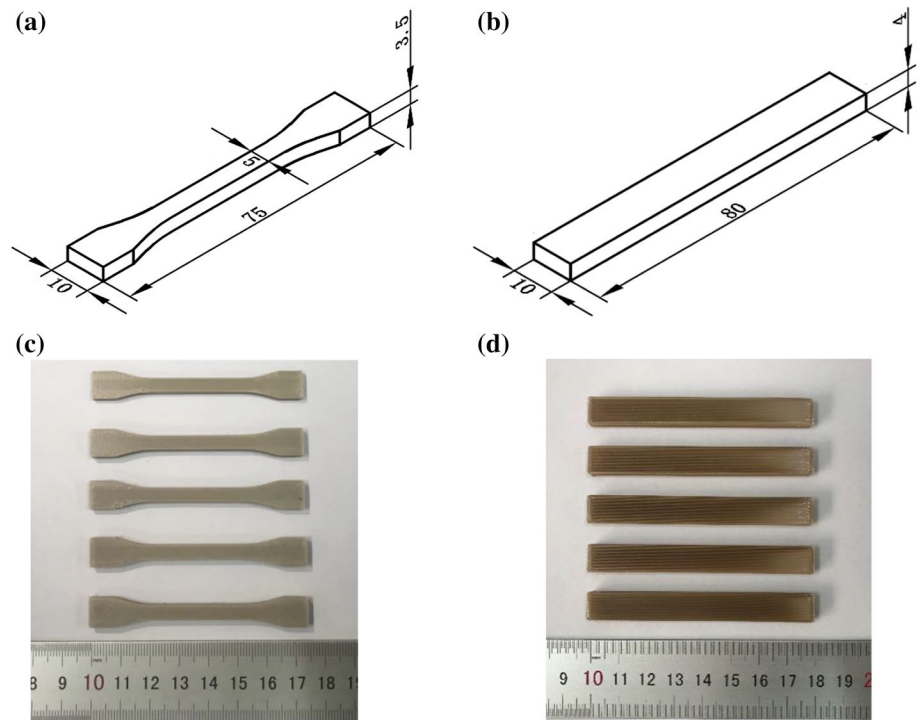
### 2.2 The Mechanical Test of 3D Printing Samples and Digital Microscope Scanning

As illustrated in Fig. 1, the mechanical tests included the interlayer bonding force (80 mm × 10 mm × 4 mm), tensile (80 mm × 10 mm × 3.5 mm), and bending strength test (80 mm × 10 mm × 4 mm). The mechanical properties were tested through ISO 527:-2:2012 and ISO 178:2001 standards, respectively, using electronic universal mechanical testing machine Instron 5982 (INSTRON, Norwood, MA, US). The interlayer bonding force was tested using three-point bending method with a loading speed of 1 mm/min, a span of 10 mm and a indenter with rounded radius 5 mm (20 mm × 10 mm × 2 mm, ISO 14130:1997) by the same mechanical testing machine Instron 5982 (INSTRON, Norwood, MA, US). The tensile strength was tested with a crosshead speed of 1 mm/min and 30 mm gauge parameter, while the bending strength was determined using a loading speed of 1 mm/min and a span of 72 mm. To ensure repeatability and preciseness of

**Table 1** 3D printing parameters configuration

Description	Dimension	Description	Dimension
Layer height	0.1 mm	Infill density	100%
Line width	0.4 mm	Infill pattern	Lines
Print speed	40 mm/s	Shell pattern	Lines
Build plate	raft	Infill line directions	0°

**Fig. 1** Standard test samples. **a** CAD of tensile bar, **b** CAD of bending bar, **c** tensile and bending test samples



all experiments, five samples were printed for each group of parameters, and the strain–stress curve was constructed using the closest date to the average results. The digital microscope VNX-6000 (KEYENCE, Singapore PTE. Ltd) was used to observe the cross-section defects and interlayer morphology of samples.

### 2.3 Thermal Property and Dynamic Mechanical Analysis

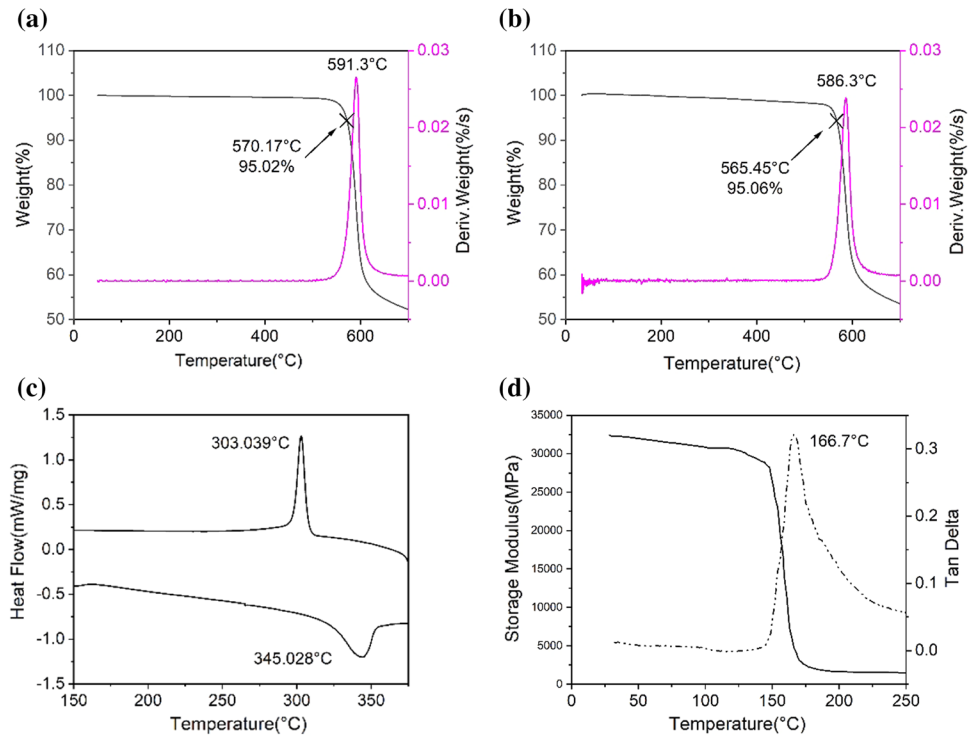
Thermogravimetric analysis (TGA) was conducted using TGA/DSC 3/1100 SF (Mettler-toledo International Inc, Switzerland). The samples were heated up to 700 °C at room temperature with a heating rate of 10 °C/min. Differential scanning calorimetry (DSC) was employed to measure the fraction of bending samples using TA DSC Q2000 (TA Instruments Inc, New Castle, US), which was heated from 23 (room temperature) to 450 °C and then cooled back to 23 °C (room temperature) at the same speed of 10°/min. Dynamic mechanical analysis (DMA) was performed using DMA+450 Dynamic mechanical analyzer (MetraviB, Limonest, France) with a sample size of 40 mm × 10 mm × 4 mm, a scanning heating rate of 5 °C/min, a frequency of 1 HZ, and an amplitude of 10 μm.

## 3 Results and Discussion

### 3.1 Raw Material and Filament Thermal Stability Analysis

Figure 2a, b showed the powder and filament TGA curves of PEEK under the same 5% weight loss at 565.45 °C and 570.17 °C, respectively, indicating that the decomposition temperature ( $T_d$ ) of filament decreased 4.72% after powder extrusion. It could be concluded that the thermal stability of filament after extrusion using a twin-screw extruder was reduced. Selecting PEEK filament as the object of this study would provide more precise results. As depicted in Fig. 2c DSC and Fig. 2d DMA, PEEK was a semi-crystalline polymer; DSC curve showed a heat absorption peak clearly at 345.028 °C, commonly referred to as the melting temperature ( $T_m$ ); however, there was no discernible heat flow at a glass transition temperature ( $T_g$ ). So, the  $T_g$  of 166.7 °C could be accurately measured using dynamic mechanical analysis of chain segments moving within the polymer. Generally, the printing temperature of nozzle should be selected from  $T_g$  to  $T_d$ . Due to incomplete plasticization of PEEK filament in low-temperature

**Fig. 2** **a** TGA curve of PEEK raw material, **b** TGA curve of PEEK filament, **c** DSC of PEEK filament, **d** DMA of PEEK sample



section, it exhibited poor fluidity and high resistance during extrusion. As a result, in this study, we selected 400 °C as the nozzle temperature.

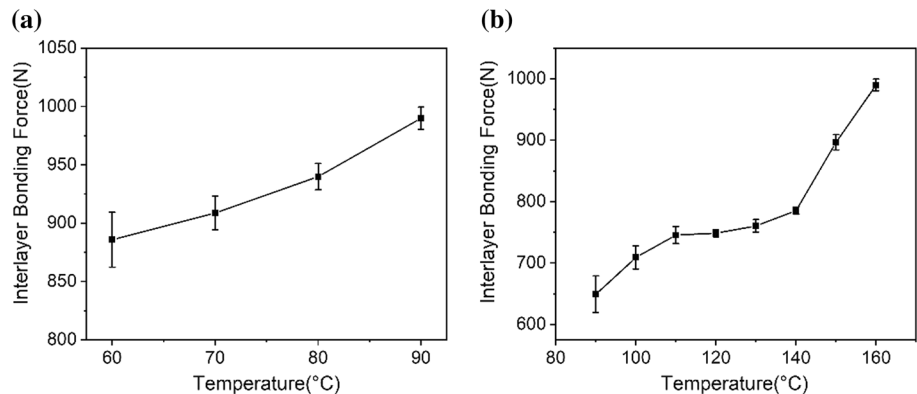
### 3.2 Effects of Temperature on Interlayer Bonding Force of PEEK Samples

At a constant bed temperature of 160 °C, four interlayer bonding force test curves were shown in Fig. 3a at ambient temperatures of 60, 70, 80, and 90 °C, respectively. The minimum interlayer bonding force was 885.87 N at 60 °C. As the ambient temperature increased, the maximum interlayer bonding force increased to 989.91 N. According to defect tendency of cross-section morphology in Fig. 4a–d, the raster became tighter as the ambient temperature increased. The

fluidity of melting material increased, and both adjacent and interlaminar rasters became closely interdiffused and entangled with each other with smaller temperature gradients and reduced cooling rates.

As known, the heating bed could prevent delamination and reduced warpage on the shrinkage of lower part, which could slow down the cooling rate. However, the heating bed could also heat the part in 3D printing process, especially the thin-thickness samples used in our study. Therefore, the initial temperature was set to 90 °C, the same as ambient temperature. When the constant ambient temperature was 90 °C, the samples were printed at bed temperature of 90 °C, 100 °C, 110 °C, 120 °C, 130 °C, 140 °C, 150 °C, and 160 °C. As depicted in Fig. 3b, changing the bed temperature significantly impacted the interlayer bonding force,

**Fig. 3** Curve of interlayer bonding forced by three-point bending test. **a** Constant bed temperature of 160 °C, the ambient temperature was from 60 to 90 °C, **b** Constant ambient temperature of 90 °C, the bed temperature was from 90 to 160 °C



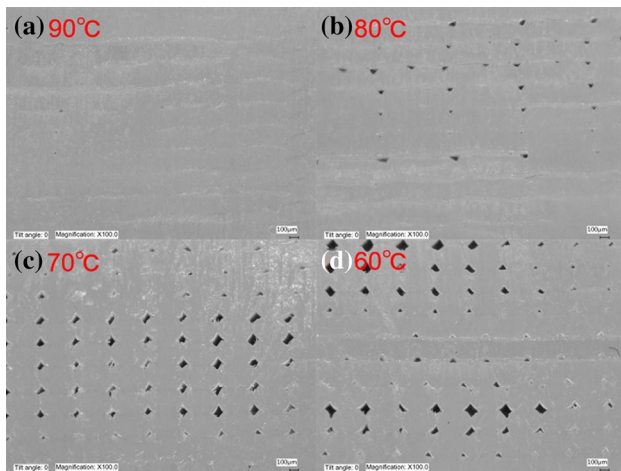
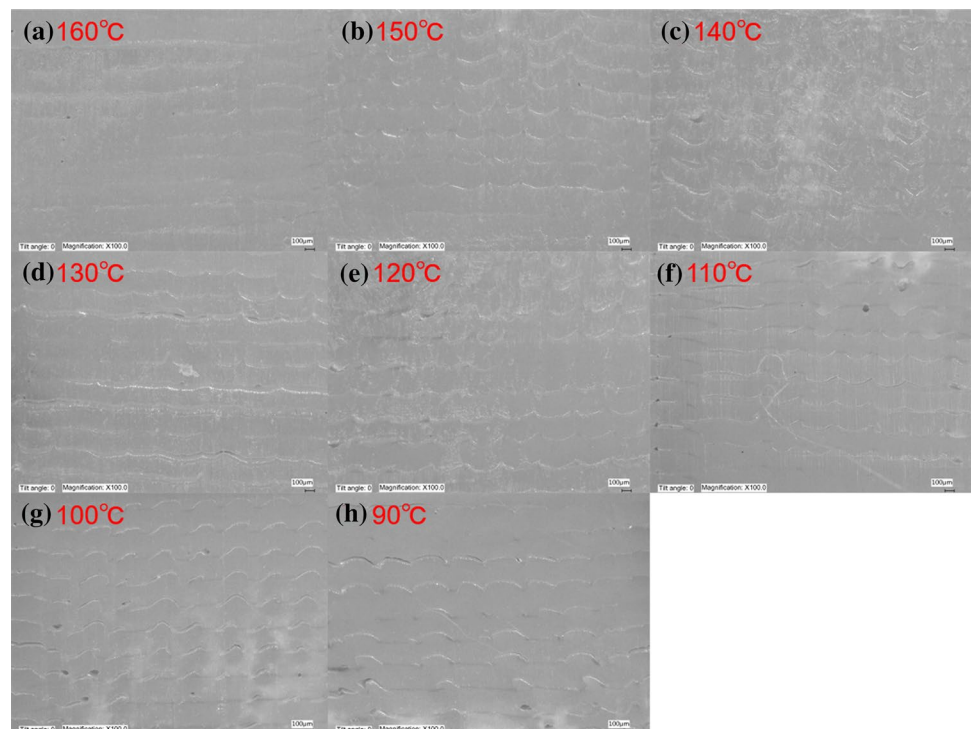


**Fig. 4** The interlayer morphology under different temperature parameters. Constant bed temperature of 160 °C, ambient temperature **a** 90 °C, **b** 80 °C, **c** 70 °C, **d** 60 °C, respectively

decreasing by 34.43% to a minimum of 649.23 N under the lowest bed condition. The printer's ability to maintain a constant ambient temperature was deteriorating, and it exported a large deviation. Compared to the first group of experiments, this one demonstrated a greater cooling temperature gradient and decreased fluidity of melting PEEK. As the bed temperature increased, the molecular chain moved faster and diffused deeper into adjacent raster in stereo space, as demonstrated by fewer bubble voids and delaminations in

**Fig. 5** The interlayer morphology under different temperature parameters. Constant ambient temperature of 90 °C, bed temperature **a** 160 °C, **b** 150 °C, **c** 140 °C, **d** 130 °C, **e** 120 °C, **f** 110 °C, **g** 100 °C, **h** 90 °C, respectively



cross-section morphology of Fig. 5e. This also demonstrated stronger interlayer bonding force and improved mechanical properties of thin-thickness samples.

### 3.3 Effects of Temperature Variations on Tensile Strength

Figure 6a displayed the tensile curve of printed specimens at 90 °C, 80 °C, 70 °C, and 60 °C under constant 160 °C of the substrate, and the tensile strengths were as follows: 86.62 MPa, 84.51 MPa, 83.06 MPa, and 81.48 MPa, which were reduced by 5.14%. Maximum pressure was reached at 90 °C compared with 100 MPa of raw material from the supplier. When the ambient temperature was dropped to 60 °C, few ladder-like shapes appeared. This was because the temperature in the top layer of the part was more affected by the ambient temperature, indicating a small temperature gradient inside. In addition, the layer force between several printing layers on the upper part of sample was relatively poor due to the low activity of internal molecular chain and increased formation of amorphous phase. Meanwhile, it could be observed that the sample delaminated initially during stretching process, initiating the breakage from the upper layer and propagating layer by layer, as previously demonstrated [21]. This could be that the bottom sample was continuously heated at a high temperature of 160 °C, resulting in a relatively higher crystallinity than the upper part. Therefore, the upper part was more brittle and prone to brittle fracture.

**Fig. 6** The stress–strain curve of the sample. **a** Curve of different ambient temperatures under substrate temperature of 160 °C, **b** curve of different substrate temperatures under ambient temperature of 90 °C, **c** tensile part fragment, **d** and tensile testing procedure

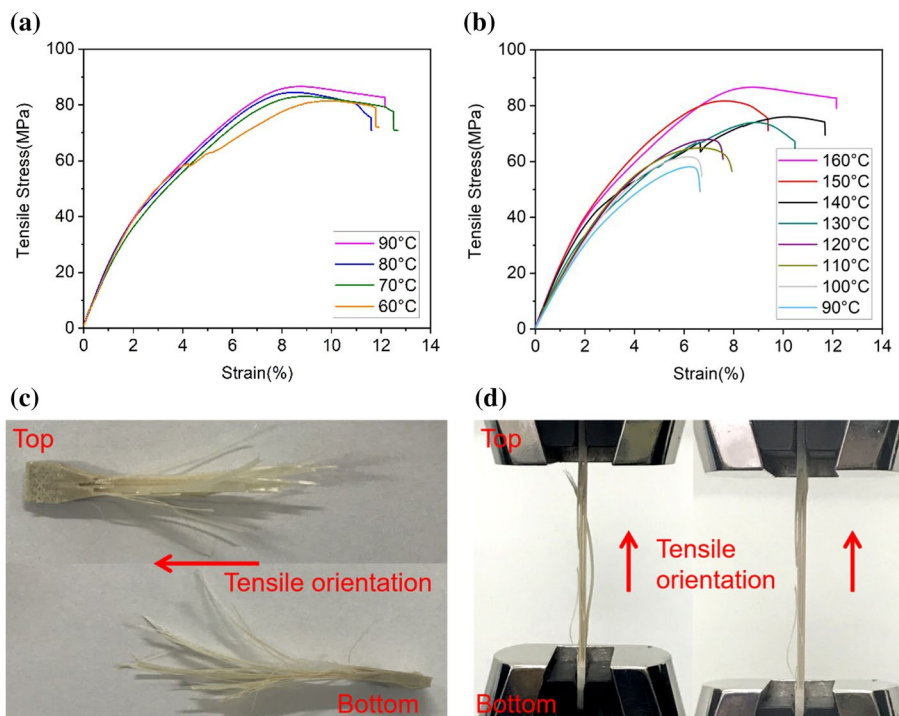


Figure 6b depicted the tensile curve when the constant temperature of chamber remained at 90 °C, and the substrate temperature decreased from 160 to 90 °C, and the tensile strengths were 86.62 MPa, 81.73 MPa, 76.06 MPa, 74.03 MPa, 67.91 MPa, 64.88 MPa, 61.68 MPa, and 58.16 MPa, respectively, with the maximum value decreased by 28.46%. Under the same ambient and substrate temperatures of 90 °C, the local high temperature was close to the nozzle, which was relatively higher than the bottom part. This led to different cooling rates and shrinkage, as well as more frequent deformation and warpage, which impacted crystallinity and interlayer bonding force. In comparison to Fig. 6a, the results indicated that variation of substrate temperature had a greater influence on the mechanical properties when printing thin-thickness PEEK samples.

In summary, increasing the substrate and ambient temperatures helped improve the mechanical performance and quality. However, due to limitations of printer's capabilities, a higher ambient field could not be achieved, but there was still room for further research.

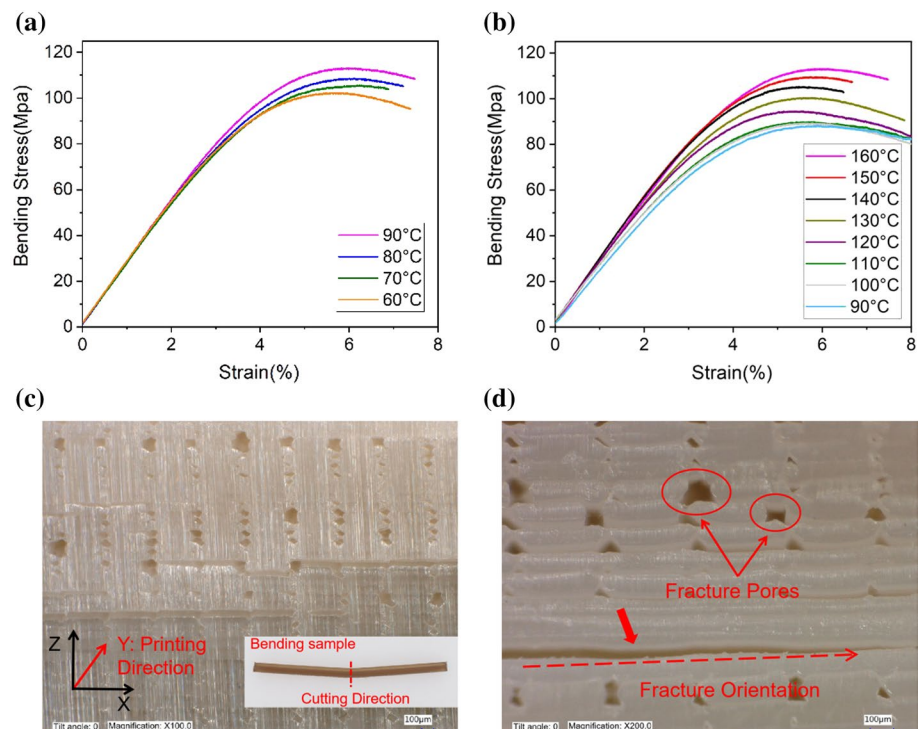
### 3.4 Effects of Temperature Variations on Bending Strength

When the substrate temperature was maintained at 160 °C, the bending stress–strain curves of different ambient temperatures were displayed in Fig. 7a, where the bending strengths were 103.96 MPa, 105.65 MPa, 108.72 MPa, and 113.21 MPa. As the ambient temperature increased,

the bending strength increased from 61.15% of the standard strength of ZYPEEK\_500G to 66.47% at room temperature of 25 °C, and the standard bending strength of ZYPEEK\_500G was known to be 170 MPa, which was 5.32% higher than that of the samples under the lowest ambient temperature. This phenomenon corroborated the tensile study results. Figure 7b displayed the experimental results at different substrate temperatures under a constant ambient temperature of 90 °C, indicating that the same bending strength variation trend could be observed. The bending strengths at 90 °C, 100 °C, 110 °C, 120 °C, 130 °C, 140 °C, 150 °C, and 160 °C were 89.42 MPa, 89.99 MPa, 94.59 MPa, 100.54 MPa, 105.32 MPa, 109.61 MPa, and 113.21 MPa, respectively, which increased by 13.86% over ZYPEEK\_550G standard bending strength under the same room temperature of 25 °C. As a result, the variation tendency was consistent with the trend when the ambient temperature increases. However, increasing the substrate temperature had a higher influence when printing thin-thickness size samples within the range of temperature control capacity by Intamsys Printer.

According to studies, increasing the temperature led to higher elastic modulus and shorter elongation, which was caused by an increase in material's crystallinity [16]. As a result of this study, it was discovered that a phenomenon could also be used to improve the interlayer bonding forces. Figure 7c, d displayed the digital microscope graph of representative sample cross-section. As could be seen, the defect between layers was relatively apparent when the substrate

**Fig. 7** Stress–strain curve of bending strength: **a** curve of different ambient temperatures under the substrate temperature of 160 °C, **b** curve of different substrate temperatures under the ambient temperature of 90 °C, **c, d** 100 and 200 times magnification of the representative cross-section under the digital microscope, the printing orientation was 0° which was perpendicular to the cross-section



temperature fell, and the orientation of printing path was perpendicular to the bending direction. The interlayer defect would initiate first and propagated along with the printing layers, demonstrating an apparent delamination effect, and then the raster of each layer continued to delaminate, gradually accumulating to the final failure. This phenomenon was also consistent with previously analyzed interlayer bonding force results.

### 3.5 Effects of Temperature Variations on Dynamic Mechanical Analysis

Figure 8 illustrated the storage modulus and lost tangent curves under two experimental conditions as used previously. As previously demonstrated, the highest storage modulus could be observed when the ambient and substrate temperatures were 90 °C and 160 °C, respectively, demonstrating that the storage modulus became higher with increasing ambient and substrate temperatures. An existing study showed that the cooling rate of extrusion material reduced when the adjacent temperature of nozzle increased, resulting in a lower cooling gradient and increased crystallinity, which restricted the activities of internal molecules and strengthened the stiffness. As known, the storage modulus of crystalline phase was much higher than the amorphous phase, improving the storage modulus of polymer. Furthermore, compared with the tensile and bending test results in Figs. 4 and 5, a tighter gap and fewer defects between rasters and interlayers were observed, and the diffusion and

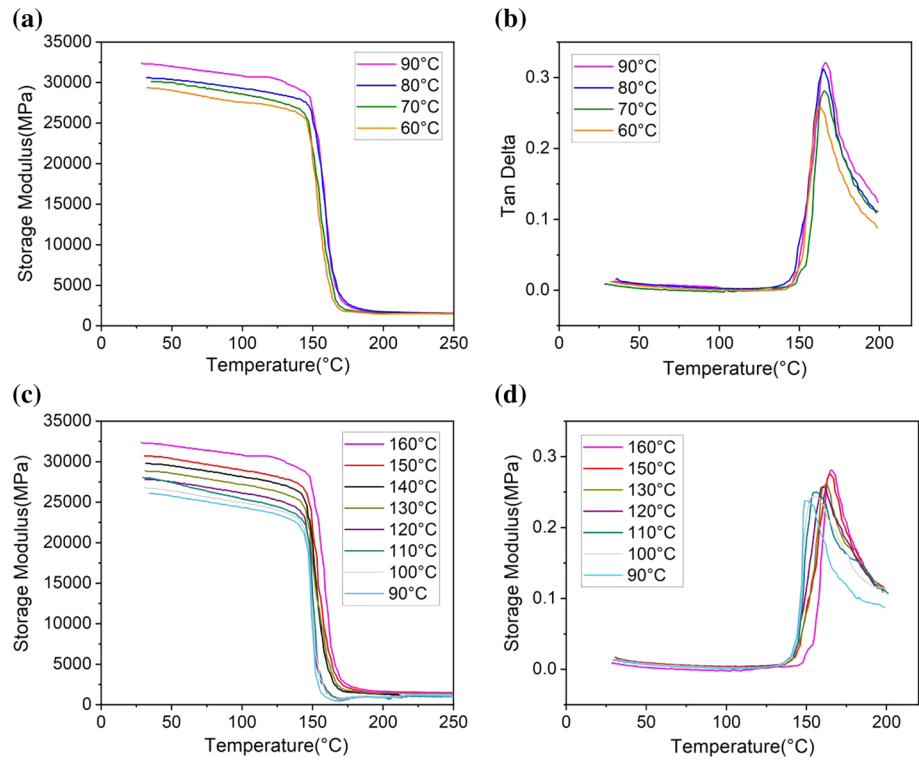
entanglement of molecular chains became much closer, which was consistent with the trend of the subsequent DSC test.

The maximum increase of storage modulus was 19.5%, and the peak of loss tangent increased 9.3%. The peak of loss tangent was the glass transition temperature ( $T_g$ ), which increased slightly from 162.3 to 165.8 °C, indicating that the molecular chain required more energy to overcome increased friction in the internal chain segment. As a result, it had a higher  $T_g$ , which meant that the samples printed at higher temperatures possessed improved toughness and shock absorption characteristics. The DMA test revealed that when printing thin-thickness samples, the substrate temperature had a greater effect on the properties and that heat transfer rate from substrate to the sample directly was greater than heat transfer rate via hot air, which could also support the conclusions of tensile and bending experiments.

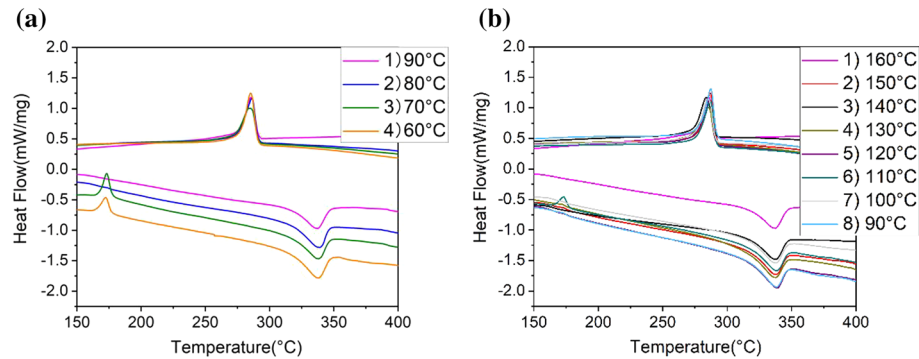
### 3.6 Effects of Temperature Variations on Crystallinity

Figure 9a illustrated the cure of printing at ambient temperatures ranging from 60 to 90 °C while maintaining a constant substrate temperature at 160 °C, as well as heating (bottom) and cooling (upper) cycles. As previously discussed, the printer's own condition made it impossible to maintain a constant ambient temperature below 60 °C under substrate temperature of 160 °C. Therefore, Table 2 contained the results of thermodynamics and crystallinity calculations for

**Fig. 8** The curve at a constant substrate temperature of 160 °C when ambient temperature increased from 60 to 90 °C, **a** storage modulus, **b** loss tangent. The curve at a constant ambient temperature of 90 °C when substrate temperature increased from 90 to 160 °C, **c** storage modulus, **d** loss tangent



**Fig. 9** DSC thermal curves. **a** Curve of different ambient temperatures under a substrate temperature of 160 °C, **b** curve of different substrate temperatures under ambient temperature of 90 °C, the melting temperature ( $T_m$ ), crystallization temperature ( $T_c$ ), as well as heat and cool flow were shown, respectively



**Table 2** Result of DSC analysis of thermal properties and crystallization on constant bed temperature

Samples	$T_m$ (°C)	$T_c$ (°C)	$\Delta H_m$ (J/g)	$\Delta H_c$ (J/g)	Crystallinity (%)
160–90	337.89	289.45	47.30	49.59	31.56
160–80	337.31	288.30	42.05	49.21	30.10
160–70	336.09	287.85	40.84	46.43	28.18
160–60	336.26	286.34	38.14	36.69	26.12

DSC test. In comparison to Fig. 9a and Table 2, the melting temperatures of DSC samples increased as ambient temperatures increased, indicating that the maximum melting temperature ( $T_m$ ) was 337.89 °C, and few DSC samples exhibited an exothermic entropy during heating process around

175 °C due to incomplete crystallization. Additionally, the same crystallization temperature ( $T_c$ ) tendency was demonstrated, with a maximum  $T_c$  of 289.45 °C.

Figure 9b showed the substrate's temperature curves for seven representative parameters ranging from 90 to 160 °C, assuming that the ambient temperature remained constant at 90 °C. The thermodynamics and crystallization obtained by DSC were summarized in Table 3. The maximum values of  $T_m$  and  $T_c$  could be observed with increasing the substrate temperature at 160 °C, confirming the previous DSC results. The crystallinity of DSC samples was calculated by  $(\Delta H_m - \Delta H_{ch}) / \Delta H_f$ , where  $\Delta H_m$  denoted endothermic entropy,  $\Delta H_{ch}$  denoted crystallized entropy in heating process, and  $\Delta H_f$  referred to as the standard of 100% crystalline PEEK material of 130 J/g.



**Table 3** Result of DSC analysis of thermal properties and crystallization on constant chamber temperature

Samples	$T_m$ (°C)	$T_c$ (°C)	$\Delta H_m$ (J/g)	$\Delta H_c$ (J/g)	Crystallinity (%)
90–160	337.89	289.45	47.30	49.59	31.56
90–150	337.21	288.77	44.79	46.48	30.19
90–140	337.85	287.94	44.76	45.85	29.17
90–130	336.99	287.15	43.83	48.28	28.46
90–120	336.76	286.73	43.40	49.96	26.13
90–110	336.59	285.21	41.43	49.96	25.63
90–100	336.46	285.27	40.47	50.14	24.89
90–90	335.95	283.72	37.84	46.85	22.81

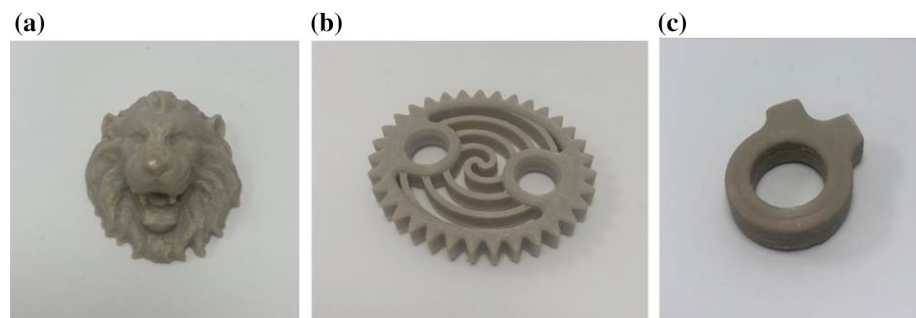
$T_m$  was the melting temperature,  $T_c$  was the crystallization temperature,  $\Delta H_m$  was the endothermic entropy of heat flow, and  $\Delta H_c$  was the exothermic entropy of cooling flow

The maximum crystallinity of the sample was 31.56%. By comparing the results in Tables 2 and 3, it could be seen that decreasing the ambient and substrate temperatures had a significant effect on printing results, resulting in a decreased crystallinity and that the substrate temperature had a significant effect on the performance of thin-thickness printing samples.

Due to its higher molecular chain, PEEK was a semi-crystalline polymer. Due to higher oriented structure of the crystalline phase, it possessed stronger mechanical properties than the amorphous phase. Slowing down the cooling rate of filament extruded from the nozzle could reduce the amorphous phase, which was consistent with DMA, tensile and bending test results.

### 3.7 PEEK Samples Printed on Optimal Temperature Parameters

The thin-thickness samples were successfully printed using the optimal ambient and substrate temperatures. As illustrated in Fig. 10, the gear, relief of lion head, and scaffold were all obtained; there was no apparent delamination, indicating high resolution and surface quality.

**Fig. 10** The samples printed with the optimal parameters

## 4 Conclusion

This study aimed to explore the influence of varying ambient and substrate temperatures on the mechanical and thermal properties of 3D-printed thin-structure PEEK components, and the experimental results indicated that printing parameters had a significant influence on the properties of the printed parts. The mechanical properties were optimal at the ambient temperature of 90 °C and a substrate temperature of 160 °C, which were within the printer's capacity. Compared with the lowest initial ambient and substrate temperature 60 °C and 90 °C, the maximum relative interlayer bonding force achieved was 989.91 N, and the maximum tensile strength was 86.62 MPa, which was 86.62% of ZYPEEK\_550G (Jilin Joinature Polymer Co., Ltd, Changchun, China) of original parameters given by the supplier, and the maximum bending strength was 66.47% of ZYPEEK\_550G, which is 113.21 MPa. The effect of substrate and ambient temperature coupling on the printing process was investigated, demonstrating that higher temperature could significantly enhance the mechanical properties. Furthermore, DMA and DSC analyses revealed that when the temperature used during the 3D printing process approached glass transition temperature ( $T_g$ ), the cooling rate of PEEK material slowed down, increasing the crystalline phase and enhancing the interlayer bonding significantly. Moreover, the molecular chain diffused and entangled more tightly between raster and layers. The influence of substrate temperature was greater than the ambient temperature while within the printer's capacities, and the optimal crystallization achieved was 31.56%. However, because the mode of the printer heating devices limited the printability of the machine, and thus there remained much work to be done to continuously improve the mechanical and thermal properties and its printability of PEEK material for 3D Printing. Future research would optimize the mechanical properties by improving the printability, process parameters, and post-treatment process. It was believed that 3D printing of PEEK materials would have a good prospect and wider applications to industry and biomedical applications.

**Acknowledgements** This research was supported by National University of Singapore Centre for Additive Manufacturing (Department of Mechanical Engineering, NUS, Singapore) and Advanced Materials Additive Manufacturing (AM)2 Lab (School of Mechanical and Aerospace Engineering, Jilin University, China).

**Author Contributions** WW, JYHF and GL provided the idea, HQ conceived the experiment process and cooperated with WZ, ZL and LH to publish it. HQ collated the data and analyzed to finish the manuscript. All authors worked together to revise and contributed to the final conclusions.

**Funding** This research was sponsored by the Key Scientific and Technological Research Project of Jilin Province (No. 20180201055GX); Project of the International Science and Technology Cooperation of Jilin Province (No. 20170414043GH); Industrial Innovation Project of Jilin Province (No.20150204037SF).

**Data Availability** This study was based only on data obtained using the methods described in this paper.

**Code Availability** Not applicable.

## Declarations

**Conflict of interest** The authors declare that they have NO known competing financial interests in the subject matter or personal relationships which have or could be perceived to have influenced the work discussed in this manuscript.

**Ethical Approval** Not applicable.

**Consent to Participate** Not applicable.

**Consent for Publication** The authors declare to participate in this study willingly, consent this paper for publication.

## References

1. Wu, W., Geng, P., Li, G., Zhao, D., Zhang, H., & Zhao, J. (2015). Influence of layer thickness and raster angle on the mechanical properties of 3D-printed PEEK and a comparative mechanical study between PEEK and ABS. *Materials*, *8*, 5834–5846.
2. Li, G., Zhao, J., Wu, W., Jiang, J., Wang, B., Jiang, H., & Fuh, J. Y. H. (2018). Effect of ultrasonic vibration on mechanical properties of 3D printing non-crystalline and semi-crystalline polymers. *Materials*, *11*, 826.
3. Zhang, Y., Li, R., Wu, W., Qing, Y., Tang, X., Ye, W., Zhang, Z., & Qin, Y. (2018). Adhesion and proliferation of osteoblast-like cells on porous polyetherimide scaffolds. *BioMed Research International*, *2018*, 7.
4. Ding, S., Zou, B., Wang, P., & Ding, H. (2019). Effects of nozzle temperature and building orientation on mechanical properties and microstructure of PEEK and PEI printed by 3D-FDM. *Polymer Testing*, *78*, 105948.
5. Wu, W., Ye, W., Geng, P., Wang, Y., Li, G., Hu, X., & Zhao, J. (2018). 3D printing of thermoplastic PI and interlayer bonding evaluation. *Materials Letters*, *229*, 206–209.
6. Geng, P., Zhao, J., WuWang, W. Y., Wang, B., Wang, S., & Li, G. (2018). Effect of thermal processing and heat treatment condition on 3D printing PPS properties. *Polymers*, *10*, 875.
7. Heidari-Rarani, M., Rafiee-Afarani, M., & Zahedi, A. M. (2019). Mechanical characterization of FDM 3D printing of continuous carbon fiber reinforced PLA composites. *Composites Part B: Engineering*, *175*, 107147.
8. Caminero, M. A., Chacón, J. M., García-Moreno, I., & Rodríguez, G. P. (2018). Impact damage resistance of 3D printed continuous fibre reinforced thermoplastic composites using fused deposition modelling. *Composites Part B: Engineering*, *148*, 93–103.
9. Yao, X., Luan, C., Zhang, D., Lan, L., & Fu, J. (2017). Evaluation of carbon fiber-embedded 3D printed structures for strengthening and structural-health monitoring. *Materials and Design*, *114*, 424–432.
10. Gonçalves, J., Lima, P., Krause, B., Pötschke, P., Lafont, U., Gomes, J. R., Abreu, C. S., Paiva, M. C., & Covas, J. A. (2018). Electrically conductive polyetheretherketone nanocomposite filaments: from production to fused deposition modeling. *Polymers*, *10*, 925.
11. Berretta, S., Davies, R., Shyng, Y. T., Wang, Y., & Ghita, O. (2017). Fused deposition modelling of high temperature polymers: Exploring CNT PEEK composites. *Polymer Testing*, *63*, 251–262.
12. Bayraktar, I., Doganay, D., Coskun, S., Kaynak, C., Akca, G., & Unalan, H. E. (2019). 3D printed antibacterial silver nanowire/poly(lactide) nanocomposites. *Composites Part B: Engineering*, *172*, 671–678.
13. Ahmed, W., Siraj, S., & Al-Marzouqi, A. H. (2020). 3D printing PLA waste to produce ceramic based particulate reinforced composite using abundant silica-sand: Mechanical properties characterization. *Polymers*, *12*(11), 2579.
14. Basgul, C., MacDonald, D. W., Siskey, R., & Kurtz, S. M. (2020). Thermal localization improves the interlayer adhesion and structural integrity of 3D printed PEEK lumbar spinal cages. *Materialia*, *10*, 100650.
15. Yuan, B., Cheng, Q., Zhao, R., Zhu, X., Yang, X., Yang, X., Zhang, K., Song, Y., & Zhang, X. (2018). Comparison of osteointegration property between PEKK and PEEK: Effects of surface structure and chemistry. *Biomaterials*, *170*, 116–126.
16. Popescua, D., Zapciua, A., Amzab, C., Baciuc, F., & Marinescu, R. (2018). FDM process parameters influence over the mechanical properties of polymer specimens: A review. *Polymer Testing*, *69*, 157–166.
17. Berretta, S., Evans, K. E., & Ghita, O. R. (2016). Predicting processing parameters in high temperature laser sintering (HT-LS) from powder properties. *Materials and Design*, *105*, 301–314.
18. Hu, B., Duan, X., Xing, Z., Xu, Z., Du, C., Zhou, H., Chen, R., & Shan, B. (2019). Improved design of fused deposition modeling equipment for 3D printing of high-performance PEEK parts. *Mechanics of Materials*, *137*, 103139.
19. Jiang, S., Liao, G., XuLiu, D. F., Li, W., Cheng, Y., Li, Z., & Xu, G. (2019). Mechanical properties analysis of polyetherimide parts fabricated by fused deposition modeling. *High Performance Polymers*, *31*(1), 97–106.
20. Wang, R., Cheng, K.-J., Advincula, R. C., & Chen, Q. (2019). On the thermal processing and mechanical properties of 3D-printed polyether ether ketone. *MRS Communications*, *9*, 1046–1052.
21. Yang, C., Tian, X., Li, D., Cao, Yi., Zhao, F., & Shi, C. (2017). Influence of thermal processing conditions in 3D printing on the crystallinity and mechanical properties of PEEK material. *Journal of Materials Processing Technology*, *248*, 1–7.
22. Lin, L., Ecke, N., Huang, M., Pei, X.-Q., & Schlarb, A. K. (2019). Impact of nanosilica on the friction and wear of a PEEK/CF composite coating manufactured by fused deposition modeling (FDM). *Composites, Part B: Engineering*, *177*, 107428.

**Publisher's Note** Springer Nature remains neutral with regard to jurisdictional claims in published maps and institutional affiliations.



**Han Qu** received the M.S. degree from Jilin University, Changchun, China, and is currently working toward a Doctoral degree in Jilin University, Changchun, China. His current research include additive manufacturing, PEEK and bioprinting. His main contributions in this paper are experimental design, experimental operation, data analysis, paper editing and proofreading.



**Guiwei Li** received the PhD degree from Jilin University, Changchun, China, and is currently working as an assistant researcher in Jilin University, Changchun, China. His current research direction is mainly bioinspired 3D/4D printing. His main contributions in this paper are ideas and data analysis.



**Wei Zhang** received the the B.S. degree from Jilin University, Changchun, China, and is currently working toward a M.S. degree in Jilin University, Changchun, China. His current research direction is mainly 3D printing of special engineering plastics. His main contributions in this paper are data analysis and paper editing.



**Jerry YH Fuh** Ph. D., National university of Singapore (NUS) Centre for Additive Manufacturing, Director, NUS Research Institute (Suzhou), Principal Investigator. He has long been comitted to 3D printing, Bio-printing, Additive manufacturing and Soft robotics. His main contributions in this paper are ideas, resources and proofreading.



**Zihan Li** received the B.S. degree from Jilin University, Changchun, China, and is currently working toward a M.S. degree in Jilin University, Changchun, China. His current research direction is mainly 3D printing of special engineering plastics. His main contributions in this paper are data analysis and paper editing.



**Wenzheng Wu** Ph. D., “Tang Ao Qing Scholar” Leading Professor of Jilin University, Doctoral Supervisor, Vice Dean of School of Mechanical and Aerospace Engineering of Jilin University. He has long been committed to advanced materials, including high-performance alloys, smart materials, polymers, composite materials, biomedical materials, and other macro and micro additive manufacturing research and their application in smart precision manufacturing, advanced manufacturing, aerospace, auto-



**Liyao Hou** received the B.S. degree from Jilin University, Changchun, China, and is currently working toward a M.S. degree in Shanghai Jiao Tong University, Shanghai, China. Her research direction include 3D printing and integration of machining and measurement. Her main contribution to this paper is the design of experiments and data processing.

otive, biomedical and other fields. His main contributions in this paper are ideas, editing, resources.